Supporting Online Material for

A Model of the Oxygen-Evolving Center of Photosystem II predicted by Structural Refinement based on EXAFS Simulations

Eduardo M. Sproviero, José A. Gascón[1], James P. McEvoy[2],

Gary W. Brudvig, and Victor S. Batista*

Department of Chemistry, Yale University, New Haven, Connecticut, 06520-8107.

Current Addresses: [1]*Department of Chemistry, University of Connecticut; Unit 3060, Storrs, CT 06269;* [2]*Department of Chemistry, Regis University, 3333 Regis Bvld., Denver, CO 80221.*

[*]To Whom Correspondence Should be Addressed: victor.batista@yale.edu;
RECEIVED DATE (automatically inserted by publisher)

This PDF file includes:

Methods and Models

Figures S1–S10.

References

Methods and Models:

QM/MM Structural Model. QM/MM molecular models were built as recently reported[1,2] by completion and structural refinement of the 1S5L X-ray crystal structure of PSII from *Thermosynechococcus elongatus*.[3] The computational models explicitly consider 1987 atoms of PSII, including the proposed Mn_3CaO_4Mn unit and all amino acid residues with α-carbons within 15 Å from any atom in the OEC metal ion cluster. Geometry optimization of the complete structural model is performed in the presence of a buffer layer of amino-acid residues with α-carbons, within 20–25 Å from any atom in region X, with harmonic constraints that preserve the natural shape of the system. The coordination of Mn ions is completed by hydration, assuming a minimum displacement of the ligating residues from their crystallographic positions and the usual coordination of five, or six, ligands to Mn ions with oxidation states III and IV, respectively. The variable coordination of calcium, typically with 6–8 ligands, was satisfied by the coordination of proteinaceous ligands, water molecules and negative counterions.

Spin Polarized and Spin Coupled Systems. The OEC metal cluster has unpaired spins, and require spin-polarized methods. These systems are also spin-coupled, including both oxomanganese complexes and metal-radical ligand interactions. The spin-coupled metal sites and/or metal-ligand radical interactions, are modeled by using spin polarized broken symmetry (BS) DFT methods.[4] In its current form, with recent density functional potentials and geometry optimization capability, BS-DFT is the most accurate approach available for these types of systems. BS-DFT also facilitates ligand field analysis for metal d→d, charge transfer (ligand→metal, metal→ligand), and intervalence charge transfer (metal→metal or ligand→ligand) transitions.

Energy Evaluation. Under the DFT QM/MM approach, the system is partitioned into a reduced system *X* (including the metal cluster and ligands) and region *Y* that includes the rest of the system. The total energy E is obtained, as recently reported,[1,2] by using the two-layer ONIOM Electronic-Embedding (EE) link-hydrogen atom method as implemented in Gaussian03:[5] $E = E^{MM,X+Y} + E^{QM,X} - E^{MM,X}$, where $E^{MM,X+Y}$ is the energy of the complete system computed at the molecular mechanics level of theory, while $E^{QM,X}$ and $E^{MM,X}$ correspond to the energy of the reduced-system *X* computed at the QM and MM levels of theory, respectively. Electrostatic interactions between regions X and Y are included in the calculation of both $E^{QM,X}$ and $E^{MM,X}$ at the quantum mechanical and molecular mechanics levels, respectively. Thus, the electrostatic interactions computed at the MM level in $E^{MM,X}$ and $E^{MM,full}$ cancel and the resulting DFT QM/MM evaluation of the total energy involves a quantum mechanical description of the polarization of the reduced system due to the electrostatic influence of the surrounding protein environment.

Protein Polarization. Polarization of the protein active sites induced by the distribution of charge in the QM layer is introduced by correcting the atomic charges of amino-acid residues in close contact with the QM layer, according to the self-consistent polarization protocol MoD-QM/MM.[6] The accuracy and capabilities of the MoD-QM/MM method have been recently demonstrated in applications to benchmark calculations of polypeptide-ligand model systems as well as in conjunction with the

Poisson-Boltzmann equation in applications to the description of protein-protein electrostatic interactions.[6]

Geometry relaxation. Relaxed DFT-QM/MM molecular structures are obtained at the ONIOM-EE (B3LYP/lacvp,6-31G(2df),6-31G:AMBER) level of theory, as recently reported.[1,2,7] Some of these earlier studies have also addressed the capabilities and limitations of DFT with hybrid density functionals, including the Becke-3-LeeYangParr (B3LYP), as applied to studies of biomimetic high-valent metal complexes.[7] The calculations combine ONIOM-EE QM/MM methodologies, implemented in Gaussian03,[5] with high-quality initial-guess spin-electronic states generated with Jaguar 5.5.[8] The combined approach exploits important capabilities of ONIOM, including both the link-hydrogen atom scheme for efficient and flexible definitions of QM layers and the possibility of modeling open-shell systems by performing Unrestricted-DFT (e.g., UB3LYP) calculations. Region Y (*i.e.*, the molecular structure beyond the QM layer) is described by the Amber MM force-field.[9]

Structural refinement based on polarized-EXAFS simulation. Refined (R)-QM/MM structural models are obtained by iteratively adjusting the molecular configuration of the cluster and directly coordinated ligands to the cluster according to a conjugate gradient optimization method, in order to minimize the mean squared deviation between the simulated and experimental polarized and isotropic EXAFS spectra. The adjustment of nuclear configurations is subject to the constraints of minimal displacements of the nuclear positions relative to the initial QM/MM configuration. The underlying computational procedure iteratively adjusts the molecular configuration of the system by conjugate gradient optimization of a scoring function defined in terms of the sum of squared deviations between calculated and experimental EXAFS spectra plus a quadratic penalty factor defined in terms of the squared deviations between the coordinates of the system and the configuration the reference DFT-QM/MM structure to ensure minimum displacements of the nuclear positions relative to a reference DFT-QM/MM structure. Upon convergence, the refined structures provide models that are maximally consistent with high-resolution polarized-EXAFS spectra and the reference QM/MM model, indicating whether the resulting refinement is within the range of error of QM/MM minimum energy configurations, or whether further improvement requires consideration of alternative ligation/protonation schemes.

Computations of isotropic-EXAFS spectra. Simulations of isotropic-EXAFS spectra are based on the computational protocol reported in our earlier work,[1,2] in accordance with previously published experimental EXAFS data.[10] The oscillatory part of the dipole transition matrix element (or EXAFS data $\chi(k)$) is obtained by using the module *FEFF83*, explicitly considering atoms within 10 Å of any metal in the OEC (except for the spectra of models I, II, IIa and III from Ref. [11] that include only the inorganic core of the OEC, in the absence of the surrounding ligands). The energy axis is converted into the momentum (k) space by using the transformation $k = [2\ m_e\ (E-E_0)]^{1/2}$ with E_0 = 6547 eV. Finally, the spectra in k-space $\chi(k)$ are multiplied by a window function $w(k)$, in order to reduce the so-called "side-loop effect" and Fourier-transformed considering the energy range from k=2.2 $Å^{-1}$ to the iron *K*-edge at 7100 eV. The function $w(k)$ is defined as a fractional cosine-squared extending over 10 eV at both k-range limits.

When comparing our isotropic-EXAFS spectra to other spectra previously reported in the literature we note that the value E_0 = 6547 eV is only slightly different from the value used by Yano et al. in Ref. [11] (E_0 = 6543 eV) , or the value reported in Ref. [12] (E_0 = 6540 eV), but significantly different from a previously reported value (E_0 = 6563 eV). Also, some of the spectra previously reported (e.g., see Fig. 2 in Ref. [12]) are consistent with our isotropic-EXAFS spectra only when assuming they were generated by using E_0 = 6564 eV (see Fig. S10) and Fourier transformed to the *r*-space by using a more reduced range (from k=3.5 $Å^{-1}$ to the iron *K*-edge at 7100 eV). The combination of a larger E_0 and a more reduced *k*-range gives FT-EXAFS spectra of comparable amplitudes for interactions at 1.8 and 2.7 Å (e.g., see Fig. 2 in Ref. [12]), while E_0 = 6547 eV and the energy range from k=2.2 $Å^{-1}$ gives FT-EXAFS spectra with more prominent amplitude for interactions at 1.8 than at 2.7 Å (e.g., see Fig. S6).

Computations of polarized-EXAFS spectra. Polarized EXAFS spectra of the PSII single crystal with the **e**-vector of the X-ray beam parallel to each crystal axis, *a*, *b*, *c* were simulated by using the *ab initio* real space Green function approach, as implemented in the programs FEFF83 and IFEFFIT.[13] These calculations are also based on the theory of the oscillatory structure due to multiple-scattering, originally proposed by Kronig,[14] and worked out in detail by Sayers,[15] Stern,[16] Lee and Pendry,[17] and Ashley and Doniach.[18] The EXAFS spectra were computed along the *a*, *b* and *c*-axes of the crystal for the OEC structure proposed by the XRD model 1S5L;[3] the empirical models proposed by Yano *et al.*,[11] the DFT-QM/MM model,[1] and the refined (R)-QM/MM model introduced in this paper.

Complete model structures suitable for simulations of polarized-EXAFS spectra along the crystal axes *a*, *b* and *c* of PSII were built by considering that PSII from *Thermosynechococcus elongatus* crystallizes as a homodimer (the two monomers are related by a non-crystallographic local C_2 axis) in the orthorhombic space group $P2_12_12_1$ with four symmetry-related dimers per unit cell. Therefore, the OEC models were positioned with the coordinates of one of the monomers and the coordinates of the companion monomer were calculated by using the local C_2 symmetry operation for the dimeric PSII. The constructed dimer was then replicated into the four symmetry related units within the orthorhombic $P2_12_12_1$ crystal unit cell. The FEFF8 calculations were performed with Debye-Waller parameters of 0.002 $Å^{-2}$. The energy axis was converted into the momentum (k) space by using E_0 = 6543.3 eV. A window function w(k), defined as a fractional cosine-square window (Hanning) with Δk=1, was applied to the k^3-weighted EXAFS data. The windowed spectra obtained in for a grid of *k*-points, equally spaced at 0.05 $Å^{-1}$ in the 3.5–11.5 $Å^{-1}$ *k*-range, were Fourier transformed (FT) to obtain the FT-amplitudes in the reduced (r) distance r-space.

DFT-QM/MM Model: Cartesian coordinates of the OEC of PSII.

Mn	27.717201	40.342304	70.656358
Mn	27.142389	39.521068	68.089129
Mn	29.231035	38.321432	69.549189
Mn	29.466173	38.670560	65.848459
O	27.584893	41.034847	69.032454
O	27.429768	38.708904	69.711816
O	29.445697	39.848942	70.547257
O	28.961550	39.502440	67.394840
Ca	29.427294	41.909503	67.917499
H	30.365816	37.947160	62.212286
C	29.891536	37.094393	63.100241
O	29.580412	35.930840	62.844780
O	29.665649	37.651986	64.325323
H	24.732742	42.337094	66.278449
C	25.385650	41.667956	67.201167
O	25.008980	41.773996	68.387357
O	26.346336	40.811393	66.771944
H	22.011116	37.717593	67.141946
C	23.066474	38.122596	67.777363
N	23.184928	38.137818	69.168230
C	24.265253	38.574926	67.305740
C	24.411324	38.617236	69.495166
N	25.080519	38.914100	68.386938
H	22.426558	38.017171	69.842318
H	24.634350	38.642319	66.305651
H	24.756419	38.751940	70.498524
H	26.786236	35.426777	67.635523
C	27.413521	36.579073	67.771303
O	28.483573	36.589198	68.529912
O	26.976762	37.617392	67.173005
H	26.471974	42.530728	73.143284
C	27.092433	42.769531	72.004788
O	26.937811	43.784334	71.338218
O	28.063086	41.821961	71.649935
H	32.231356	43.981411	70.647550
C	30.941345	44.006928	70.339933
O	30.341564	43.104372	69.672024
O	30.260000	45.004708	70.784014
H	31.158048	35.353672	71.652620
C	30.202990	35.781592	70.870228
O	29.593574	36.860560	71.118267
O	29.975561	35.037872	69.793299
O	31.206515	40.013004	65.356878
H	30.786318	40.936532	65.075310

H	31.847304	39.738117	64.635511
O	30.832207	37.669231	66.766055
H	31.071539	37.938878	67.894601
H	30.767817	36.638690	66.760598
O	31.087397	38.120739	69.121142
H	31.746420	38.799206	69.486289
O	25.759352	40.848589	70.638735
H	25.422445	41.239819	69.729917
H	24.973204	40.636480	71.248819
O	27.423305	39.256188	72.379436
H	27.003164	38.339305	72.234103
H	28.173367	39.167865	73.028742
O	31.726858	41.095196	67.799121
H	32.029797	42.046116	67.538412
H	31.812109	40.582636	66.911208
O	27.894536	39.612247	65.021083
H	27.907973	39.920706	64.064328
H	29.251822	35.517565	69.196120

R-QM/MM Model: Cartesian coordinates of the OEC of PSII.

Mn	27.719096	40.324994	70.662066
Mn	27.154848	39.577530	68.085572
Mn	29.241875	38.497888	69.545791
Mn	29.411008	38.504533	65.872080
O	27.570362	41.102889	69.040704
O	27.397014	38.667891	69.650279
O	29.507074	39.670086	70.538617
O	29.077257	39.468969	67.374663
Ca	29.327465	42.045220	67.977228
H	30.834880	38.232688	62.314986
C	30.343478	37.341516	63.154604
O	30.088857	36.174856	62.854639
O	30.030752	37.859322	64.378057
H	24.725863	41.603032	65.923863
C	25.402778	41.071717	66.916301
O	24.968091	41.223206	68.077452
O	26.460917	40.289280	66.586161
H	22.124428	37.796467	66.728347
C	23.144902	38.179513	67.430825
N	23.187586	38.156898	68.825972
C	24.368929	38.638910	67.037362
C	24.395846	38.621832	69.231832
N	25.125221	38.945282	68.169989
H	22.393316	38.021644	69.454395
H	24.792073	38.731429	66.060970
H	24.686275	38.728022	70.255716
H	26.858621	35.696415	67.380506

C	27.498420	36.824865	67.619193
O	28.516539	36.769516	68.444403
O	27.122425	37.903538	67.051812
H	26.321294	42.541761	73.116212
C	27.006318	42.792246	72.017953
O	26.907458	43.824240	71.367367
O	27.975833	41.832647	71.693630
H	31.900100	44.221351	70.857320
C	30.628991	44.168401	70.481976
O	30.123595	43.236274	69.777590
O	29.863306	45.116900	70.895600
H	30.845643	35.160938	71.764961
C	29.947737	35.627207	70.938074
O	29.367636	36.727615	71.160944
O	29.746759	34.896152	69.847299
O	31.355377	39.581327	65.508014
H	31.092878	40.563970	65.235517
H	31.985203	39.230442	64.810344
O	30.929183	38.060317	66.599120
H	31.089894	38.163057	67.768402
H	30.824564	37.044441	66.446662
O	31.085150	38.085371	69.233303
H	31.728106	38.752814	69.644507
O	25.633962	40.805795	70.482593
H	25.342619	41.212759	69.564980
H	24.818270	40.575544	71.045491
O	27.244482	39.211352	72.321716
H	26.812014	38.305783	72.144986
H	27.958120	39.099495	73.007429
O	31.787764	41.267155	68.018372
H	32.073653	42.234482	67.802649
H	31.938312	40.784939	67.122169
O	28.096341	39.502426	65.037021
H	28.157400	39.799905	64.078642
H	29.072384	35.404811	69.217211

Table S1. Interatomic distances in the R-QM/MM model of the OEC of PSII, using the atomic labels indicated in Fig. S1.

Atom Pair	Distances [Å]
1-2	2.74
1-3	2.63
1-5	1.80
1-6	1.97
1-7	1.91
1-34	1.84
1-51	2.14
1-54	2.05
2-3	2.77
2-4	3.34
2-5	1.85
2-6	1.83
2-8	2.05
2-9	3.29
2-17	1.80
2-23	2.13
2-30	1.97
3-4	3.68
3-6	1.86
3-7	1.56
3-8	2.38
3-9	3.88
3-29	2.17
3-41	2.40
3-49	1.91
4-8	1.82
4-13	1.74
4-43	2.25
4-46	1.74
4-60	1.85

Figures:

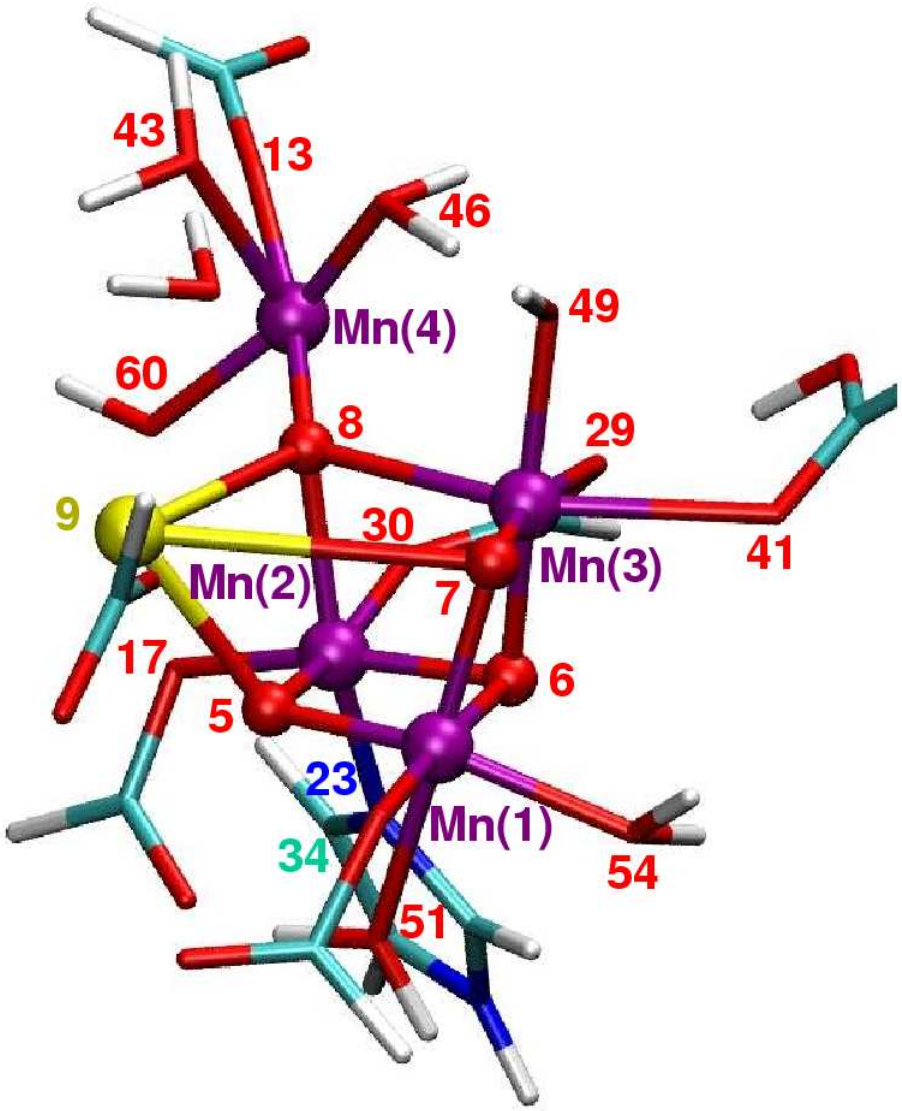

Figure S1: R-QM/MM model of the OEC of PSII including only the centers that are most relevant to calculations of EXAFS spectra.

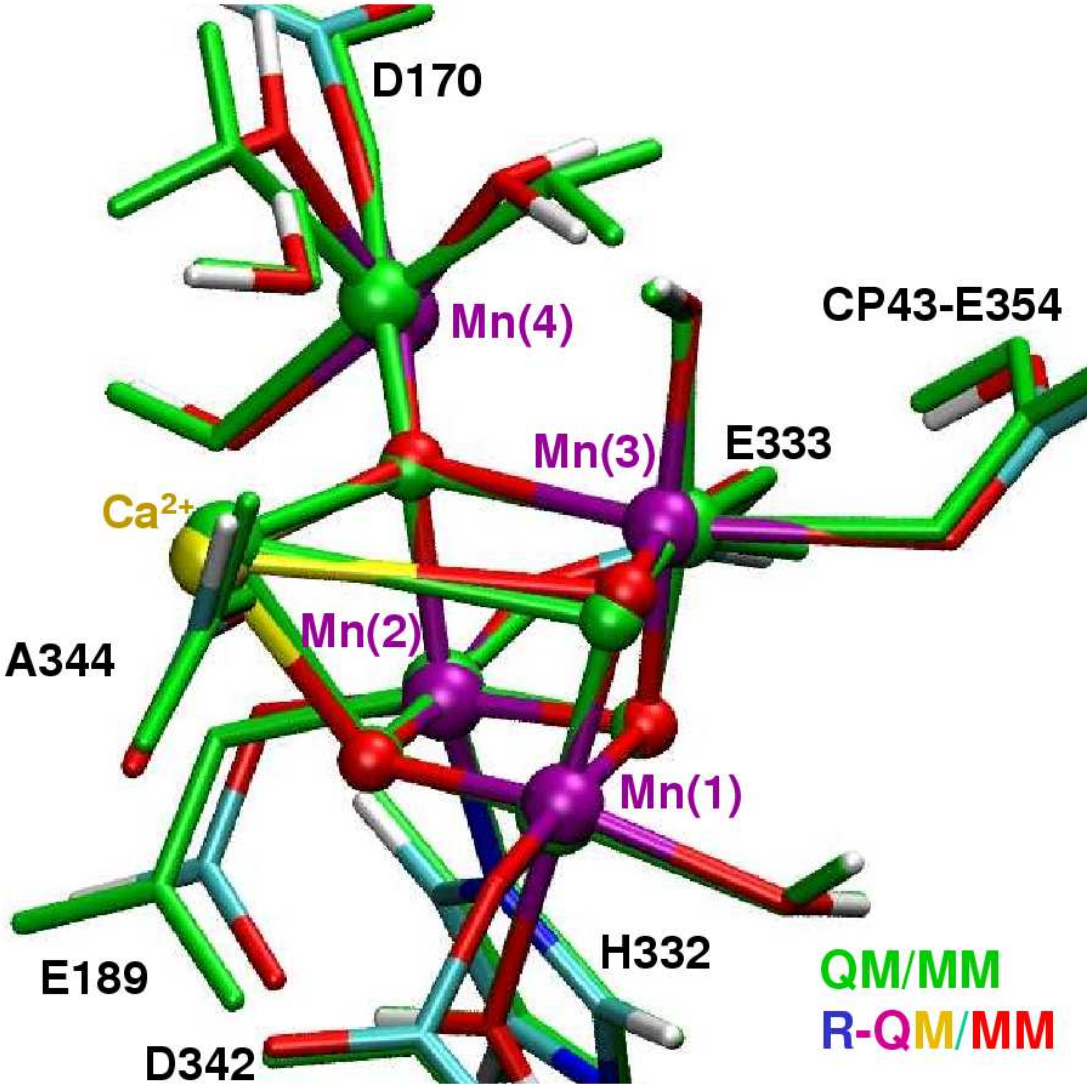

Figure S2: Superposition of the DFT-QM/MM model (green)[1,2] and the R-QM/MM (color) model of the OEC of PSII introduced in this paper.

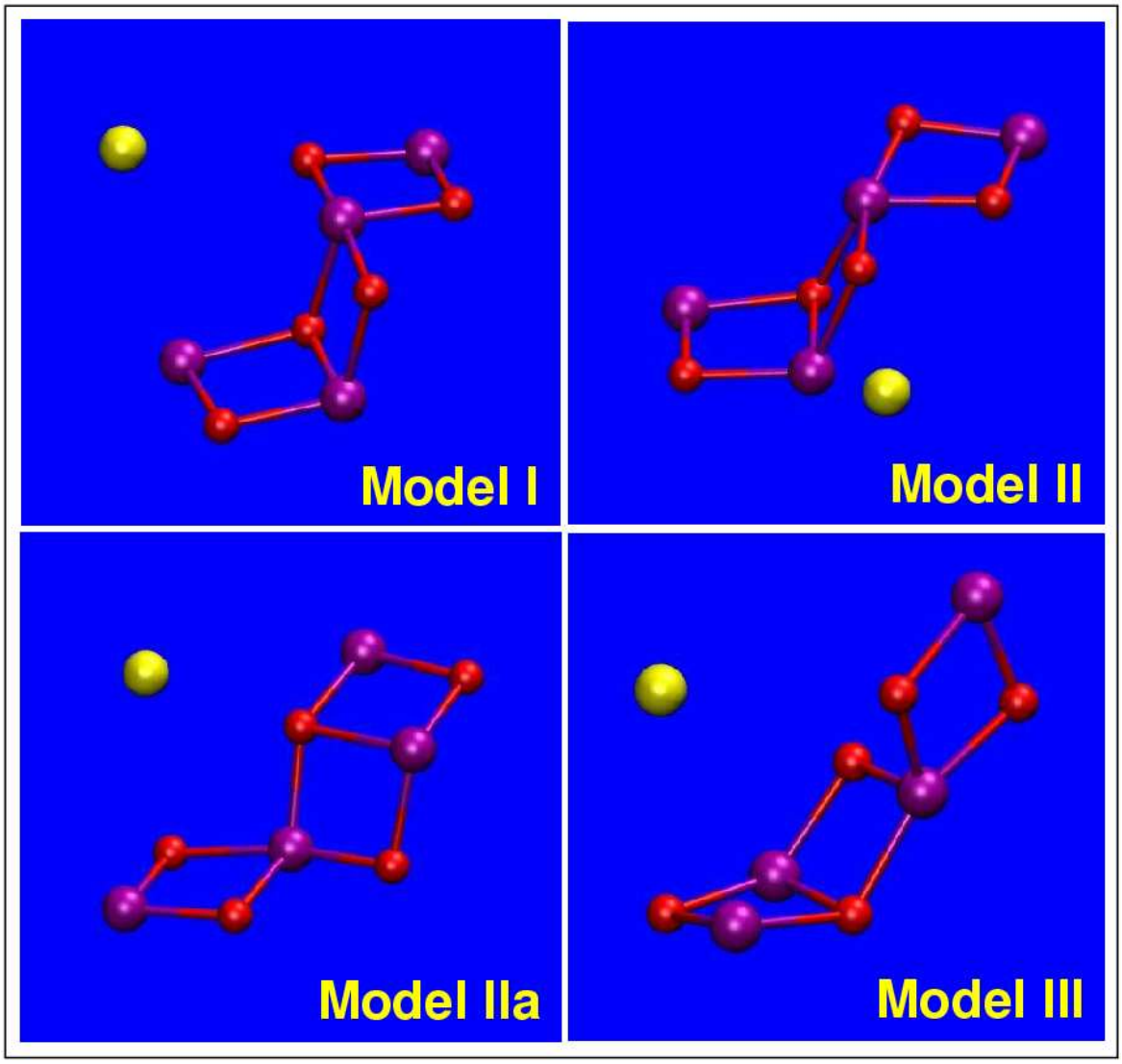

Figure S3: Empirical models of the OEC of PSII proposed by Yano et al.[11]

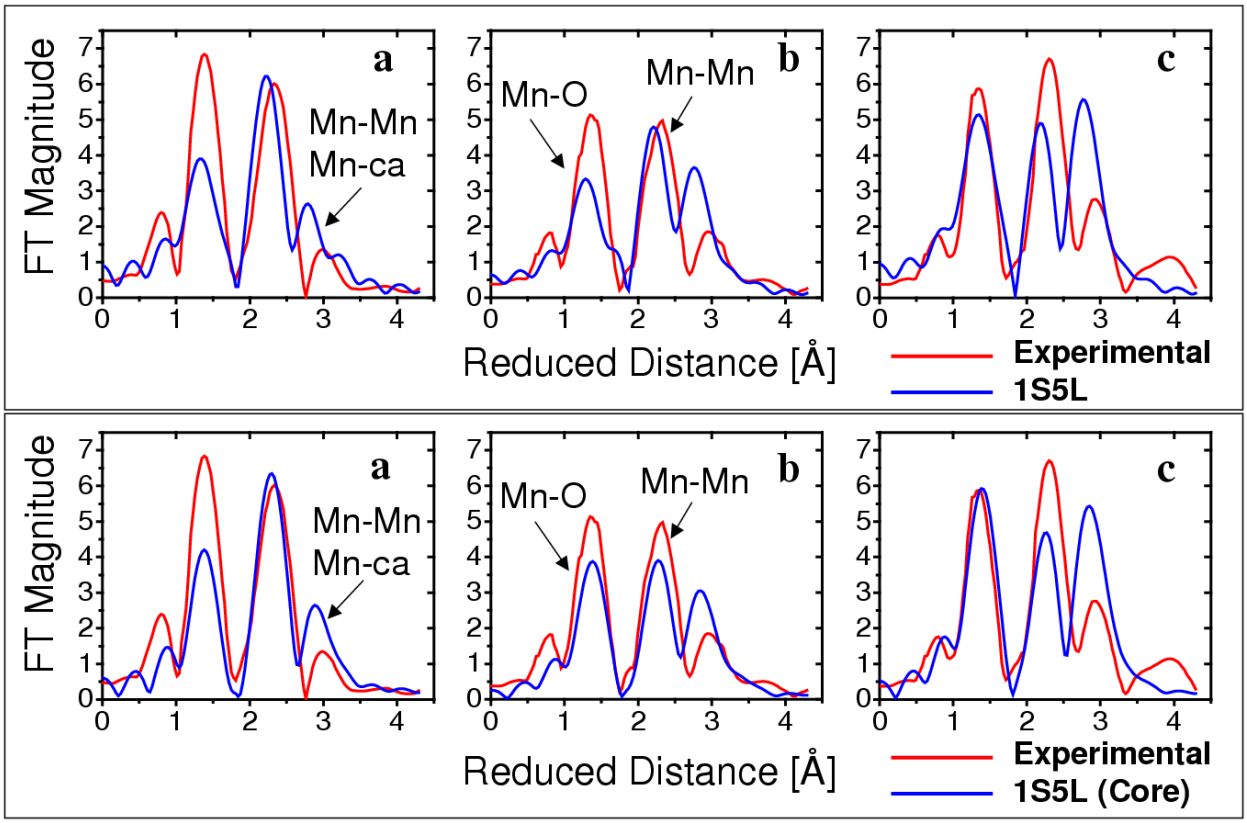

Figure S4: Comparison of the polarized-EXAFS spectra (red),[11] along the crystal axes *a*, *b* and *c*, and the corresponding spectra calculated, as described in the text, by using the coordinates of the XRD model 1S5L (blue).[3] Top and bottom panels compare the calculated spectra obtained by including (top), or neglecting (bottom), the contributions of scattering paths from the proteinaceous ligands. The deviations between calculated and experimental spectra suggest inaccuracies in distances/orientations of metal-metal, or metal-ligand vectors in the 1S5L model. In addition, the calculated EXAFS spectra (blue lines) are similar for the complete 1S5L model (top) and the 1S5L core in the absence of proteinaceous ligands (bottom), indicating that the predominant contributions to the spectra indeed result from scattering paths of the inorganic core, including scattering paths from the metal centers and oxo bridges in the Mn_3CaO_4Mn unit. At the same time, these results indicate that electron scattering paths from the ligands also introduce significant contributions to the spectra since the blue lines in the top and bottom panels are slightly different (compare overall amplitudes of the first and second peaks in top and bottom panels). Therefore, realistic simulations of EXAFS spectra of the OEC of PSII must include a complete and reliable description of the ligands coordinated to the metal cluster.

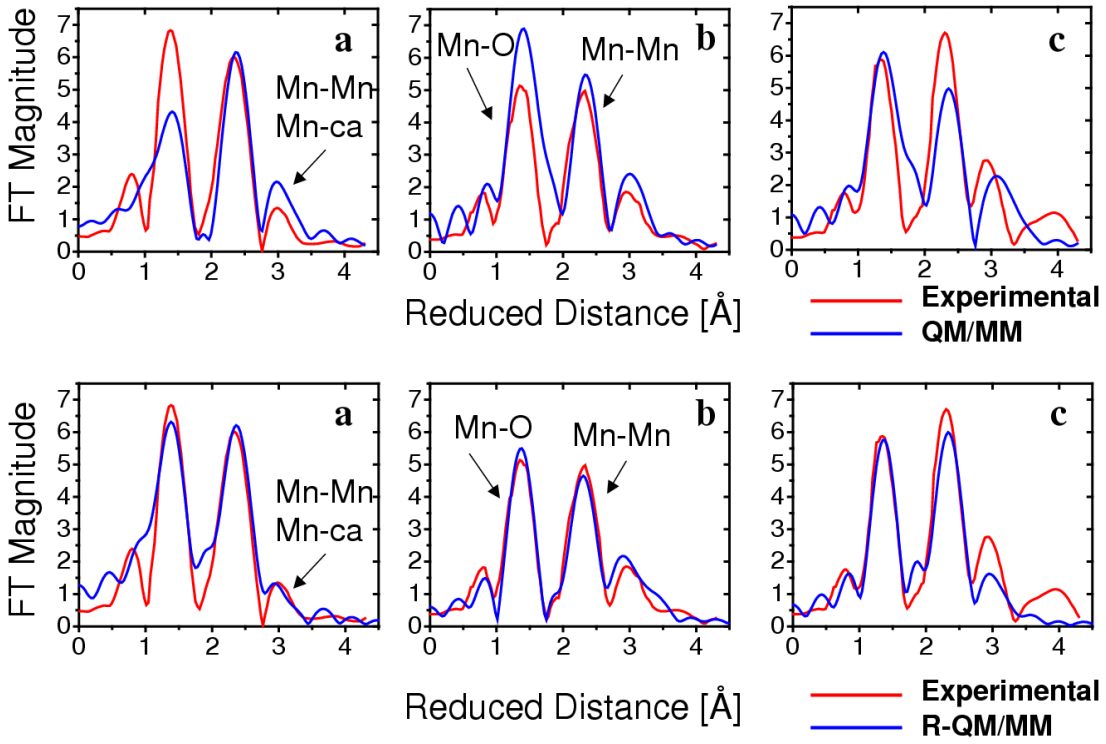

Figure S5: Comparison between polarized-EXAFS spectra (red)[11] of the OEC of PSII, along the crystal unit cell axes *a*, *b* and *c*, and the corresponding spectra calculated as described in the text (blue) by using the coordinates of the QM/MM[1,2] and R-QM/MM models (this paper). These results show that the R-QM/MM model adequately describes the polarized-EXAFS experimental data.

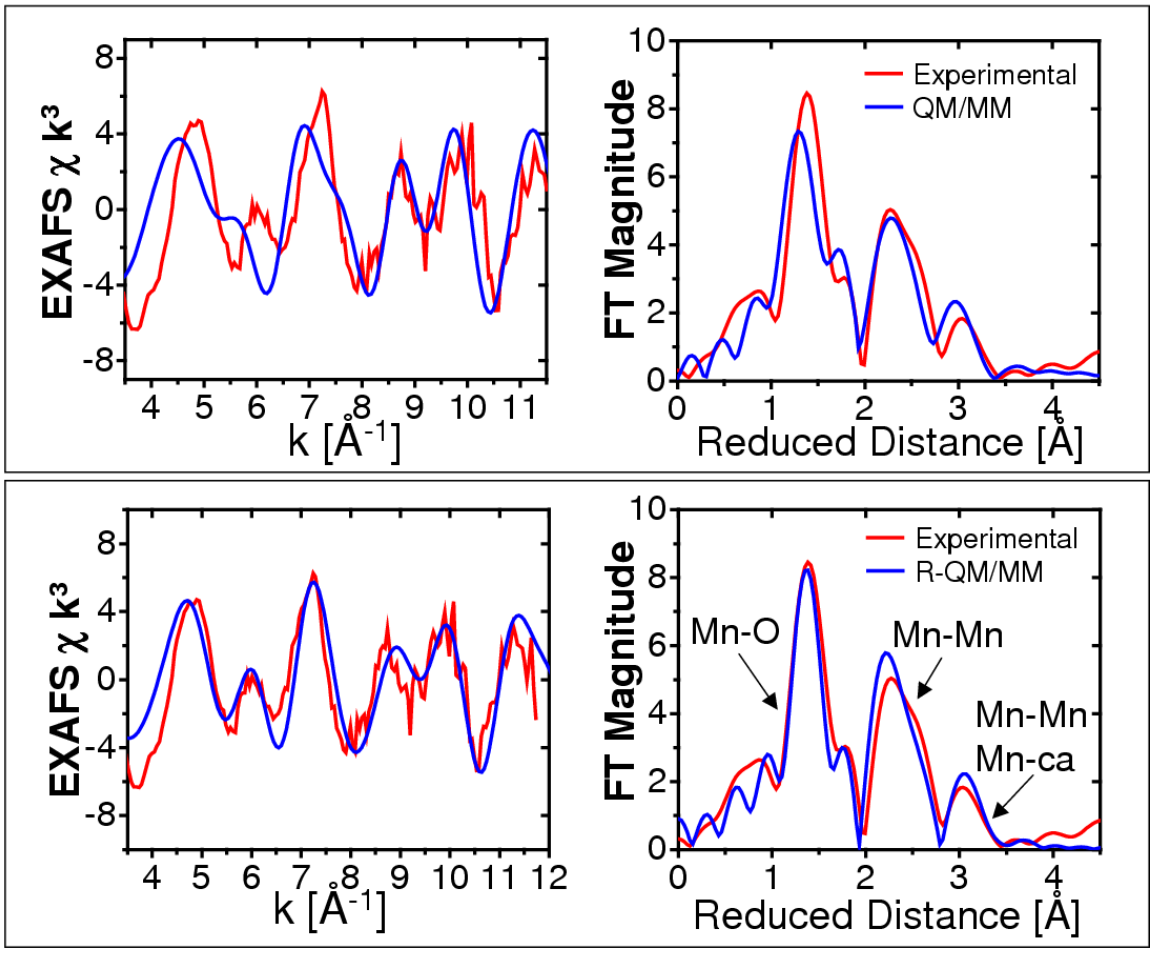

Figure S6: Comparison of the experimental isotropic EXAFS spectrum[10] and FT EXAFS Magnitude[10] (red) and the calculated spectra (blue) obtained with the QM/MM (top)[1,2] and R-QM/MM (bottom) models. These results show that the R-QM/MM structure reproduces the isotropic EXAFS experimental data, in addition to reproducing the polarized-EXAFS amplitudes along the crystal axes *a*, *b* and *c* (see Fig. S5).

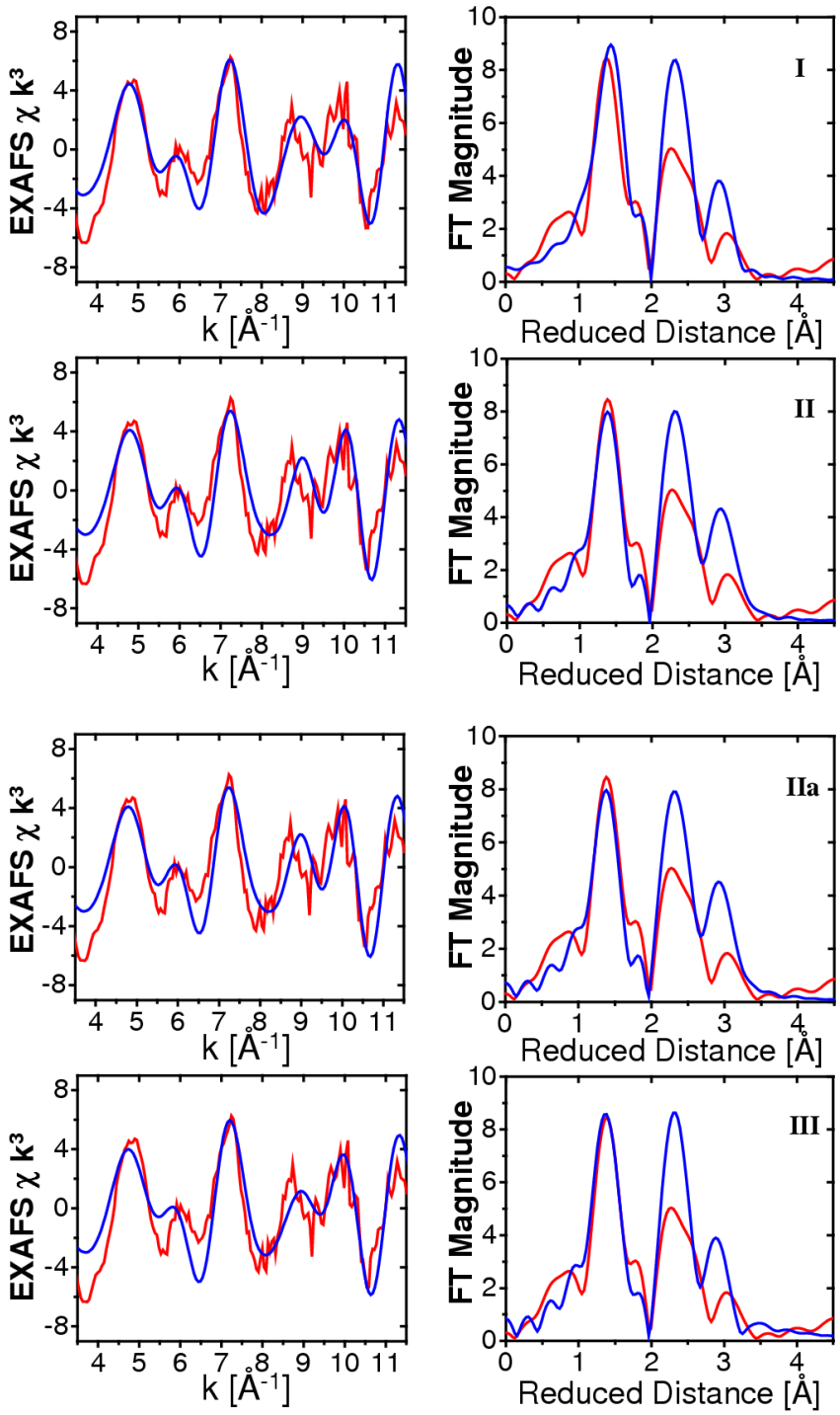

Figure S7: Isotropic EXAFS data (red)[10] compared to the calculated spectra (blue) obtained by using the four empirical models of the inorganic core proposed by Yano *et al.*[11] These results indicate that the models I, II, IIa and III adequately describe the positions of the first and second peaks, although the relative heights of the peaks are not properly described. Furthermore, the third peak is predicted to be at slightly shorter distances, according to the simulation protocol implemented in this paper.

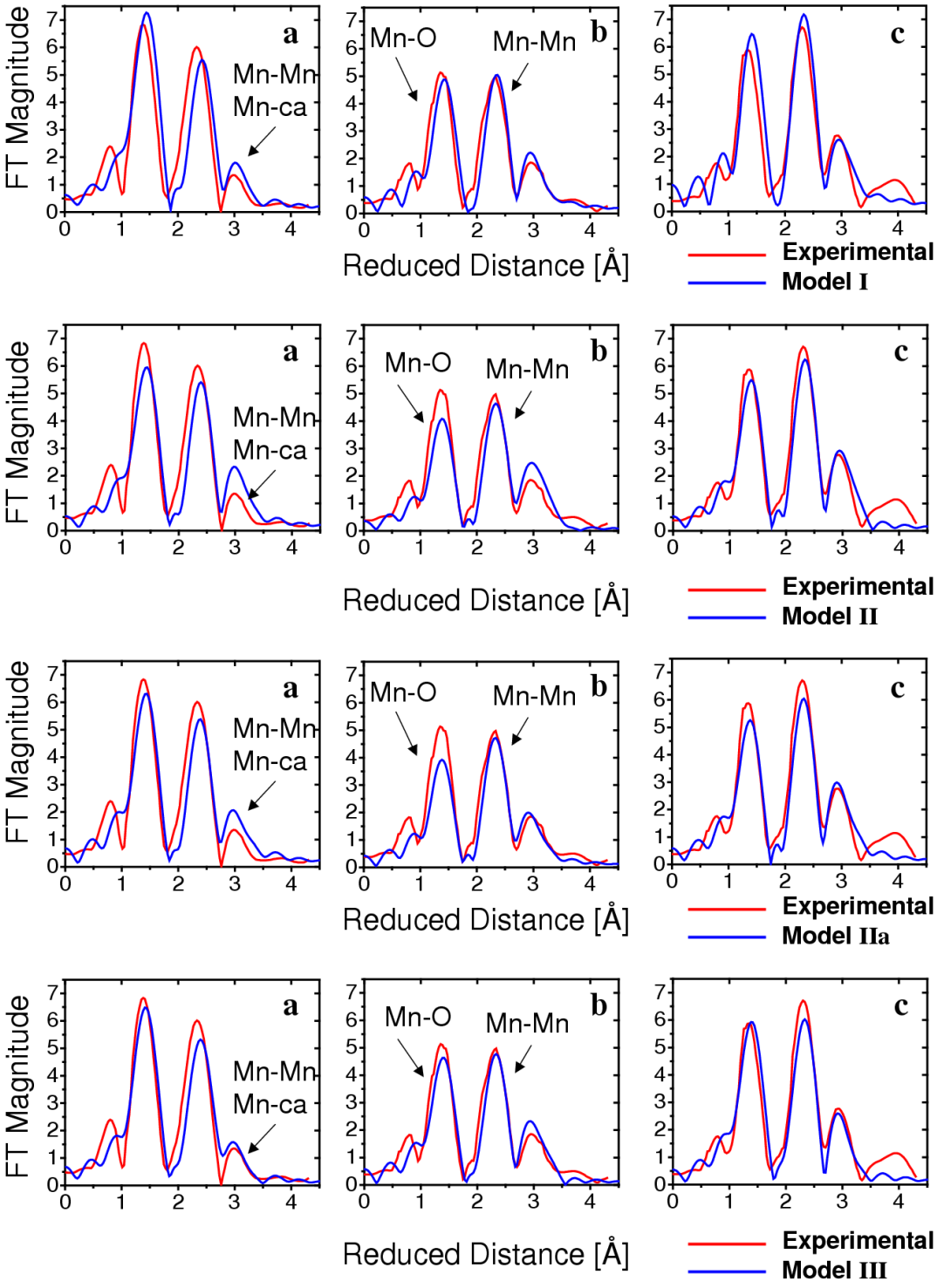

Figure S8: Comparison between the experimental polarized EXAFS spectra (red),[11] along the crystal unit cell axes *a*, *b* and *c*, and the corresponding spectra calculated as described in the text (blue) by using the coordinates of the four empirical models proposed by Yano *et al.*[11] These results show that the four models adequately describe the polarized-EXAFS spectra.

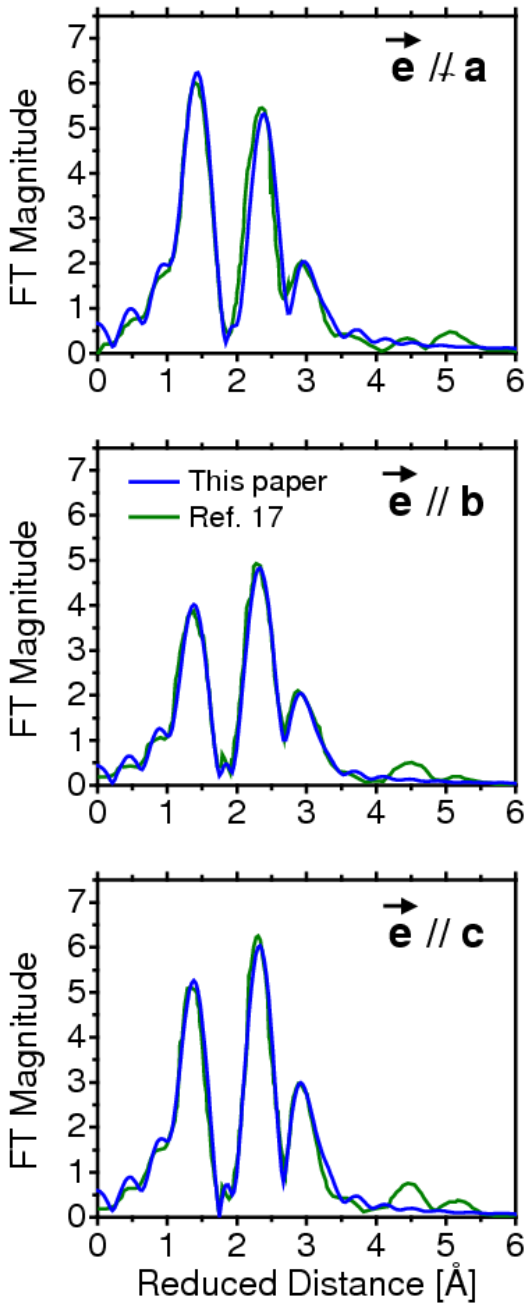

Figure S9: Comparison of the calculated polarized-EXAFS spectra reported in Ref. [11] (green lines) for model IIa, along the crystal axes *a*, *b* and *c*, and the corresponding spectra calculated as described in the text (blue lines). These results indicate that the computational protocol implemented in our studies reproduces the calculations reported in Ref [11].

(a)

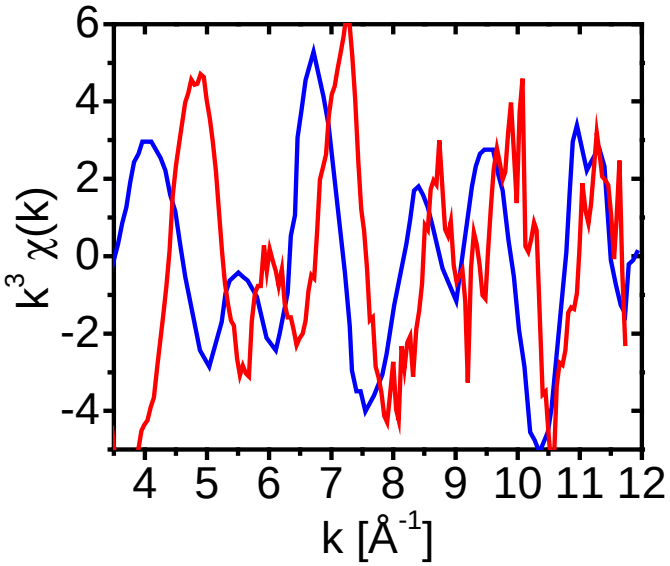

(b)

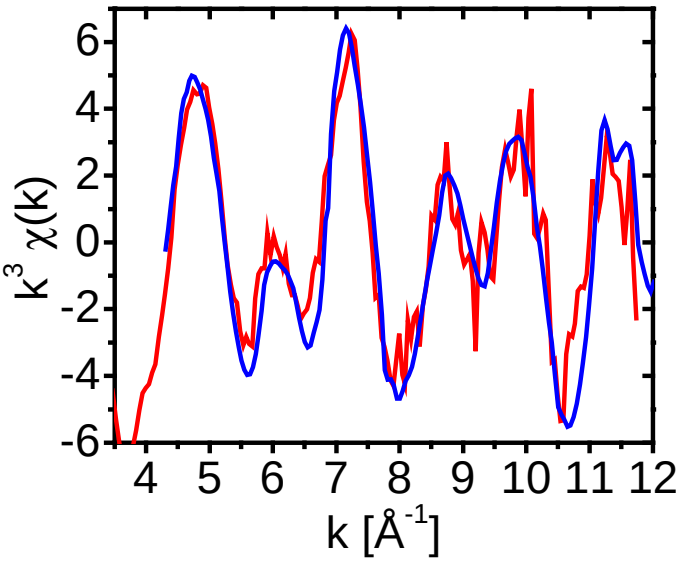

Figure S10: (a) Comparison of isotropic-EXAFS spectra reported in Ref. [12] (blue), and the corresponding experimental data, used in our computational studies, obtained Dau and co-workers.[10] (b) Same comparison presented in (a) but after transforming the data $\chi(k)$ from Ref. [12] into $\chi(E)$, using the transformation $E=E_0+k^2/(2\ m_e)$ with E_0=6564 eV and subsequently transforming the resulting spectra back to *k*-space using E_0=6547 eV. These results suggest that the spectra reported in Ref. [12] (Fig. 2) are consistent with our isotropic-EXAFS spectra only when assuming they were generated by using E_0 = 6564 eV.

References:

1 E. M. Sproviero, J. A. Gascon, J. P. McEvoy, G. W. Brudvig, and V. S. Batista, J. Chem. Theor. Comput. **2**, 1119 (2006).

2 E. M. Sproviero, J. A. Gascon, J. P. McEvoy, G. W. Brudvig, and V. S. Batista, Curr. Op. Struct. Biol. **17**, 173 (2007); E. M. Sproviero, J. A. Gascon, J. P. McEvoy, G. W. Brudvig, and V. S. Batista, J. Am. Chem. Soc. **130**, 3428 (2008); E. M. Sproviero, K. Shinopoulos, J. A. Gascon, J. P. McEvoy, G. W. Brudvig, and V. S. Batista, Phil. Trans. Royal Soc. London Series B - Biol. Sci. **363**, 1149 (2008); E. M. Sproviero, J. A. Gascon, J. P. McEvoy, G. W. Brudvig, and V. S. Batista, Coord. Chem. Rev. **252**, 395 (2008).

3 K. N. Ferreira, T. M. Iverson, K. Maghlaoui, J. Barber, and S. Iwata, Science **303** (5665), 1831 (2004).

4 L. Noodleman, J. Chem. Phys. **74**, 5737 (1981); L. Noodleman and E. R. Davidson, Chem. Phys. **109**, 131 (1986); L. Noodleman and D. A. Case, Adv. Inorg. Chem. **38**, 423 (1992); L. Noodleman, C. Y. Peng, D. A. Case, and J. M. Mouesca, Coord. Chem. Rev. **144**, 199 (1995).

5 M. J. Frisch, G. W. Trucks, H. B. Schlegel, G. E. Scuseria, M. A. Robb, J. R. Cheeseman, J. A. M. Jr., T. Vreven, K. N. Kudin, J. C. Burant, J. M. Millam, S. S. Iyengar, J. Tomasi, V. Barone, B. Mennucci, M. Cossi, G. Scalmani, N. Rega, G. A. Petersson, H. Nakatsuji, M. Hada, M. Ehara, K. Toyota, R. Fukuda, J. Hasegawa, M. Ishida, T. Nakajima, Y. Honda, O. Kitao, H. Nakai, M. Klene, X. Li, J. E. Knox, H. P. Hratchian, J. B. Cross, C. Adamo, J. Jaramillo, R. Gomperts, R. E. Stratmann, O. Yazyev, A. J. Austin, R. Cammi, C. Pomelli, J. W. Ochterski, P. Y. Ayala, K. Morokuma, G. A. Voth, P. Salvador, J. J. Dannenberg, V. G. Zakrzewski, S. Dapprich, A. D. Daniels, M. C. Strain, O. Farkas, D. K. Malick, A. D. Rabuck, K. Raghavachari, J. B. Foresman, J. V. Ortiz, Q. Cui, A. G. Baboul, S. Clifford, J. Cioslowski, B. B. Stefanov, G. Liu, A. Liashenko, P. Piskorz, I. Komaromi, R. L. Martin, D. J. Fox, T. Keith, M. A. Al-Laham, C. Y. Peng, A. Nanayakkara, M. Challacombe, P. M. W. Gill, B. Johnson, W. Chen, M. W. Wong, C. Gonzalez, and J. A. Pople, (2003).

6 J. A. Gascon, S. S. F. Leung, E. R. Batista, and V. S. Batista, J. Chem. Theory Comput. **2** (1), 175 (2006).

7 E. M. Sproviero, J. A. Gascon, J. P. McEvoy, G. W. Brudvig, and V. S. Batista, J. Inorg. Biochem. **100**, 786 (2006).

8 L. L. C. Jaguar 5.5. Schroedinger, Portland, OR., (1991-2003).

9 W. D. Cornell, P. Cieplak, C. I. Bayly, I. R. Gould, K. M. Merz, D. M. Ferguson, D. C. Spellmeyer, T. Fox, J. W. Caldwell, and P. A. Kollman, J. Am. Chem. Soc. **117** (19), 5179 (1995); W. D. Cornell, P. Cieplak, C. I. Bayly, I. R. Gould, K. M. Merz, D. M. Ferguson, D. C. Spellmeyer, T. Fox, J. W. Caldwell, and P. A. Kollman, J. Am. Chem. Soc. **118** (9), 2309 (1996).

10 M. Haumann, C. Muller, P. Liebisch, L. Iuzzolino, J. Dittmer, M. Grabolle, T. Neisius, W. Meyer-Klaucke, and H. Dau, Biochemistry **44** (6), 1894 (2005); H. Dau, P. Liebisch, and M. Haumann, Phys. Chem. Chem. Phys. **6** (20), 4781 (2004).

11 J. Yano, J. Kern, K. Sauer, M. J. Latimer, Y. Pushkar, J. Biesiadka, B. Loll, W. Saenger, J. Messinger, A. Zouni, and V. K. Yachandra, Science **314**, 821 (2006).

12 J. Yano, Y. Pushkar, P. Glatzel, A. Lewis, K. Sauer, J. Messinger, U. Bergmann, and V. K. Yachandra, J. Am. Chem. Soc. **127**, 14974 (2005).

13 A. L. Ankudinov, C. E. Bouldin, J. J. Rehr, J. Sims, and H. Hung, Physical Review B **65** (10) (2002); C. Bouldin, J. Sims, H. Hung, J. J. Rehr, and A. L. Ankudinov, X-Ray Spectrometry **30** (6), 431 (2001).

[14] R. D. Kronig, Proceedings of the Royal Society of London Series a-Containing Papers of a Mathematical and Physical Character **133** (821), 255 (1931); R. D. Kronig and W. G. Penney, Proceedings of the Royal Society of London Series a-Containing Papers of a Mathematical and Physical Character **130** (814), 499 (1931).

[15] D. E. Sayers, E. A. Stern, and F. W. Lytle, Phys. Rev. Lett. **27** (18), 1204 (1971).

[16] E. A. Stern, Phys. Rev. B **10** (8), 3027 (1974).

[17] P. A. Lee and J. B. Pendry, Phys. Rev. B **11** (8), 2795 (1975).

[18] C. A. Ashley and S. Doniach, Physical Review B **11** (4), 1279 (1975).